PHYSICS

Entangled measurement for *W* states

Geobae Park[1], Holger F. Hofmann[2], Ryo Okamoto[1,3], Shigeki Takeuchi[1,3]*,

Entangled measurements are an indispensable tool for quantum information processing, such as Bell-state measurements in quantum teleportation and entanglement swapping. However, to date, the realization of entangled measurements has mainly focused on bipartite systems or Greenberger-Horne-Zeilinger (GHZ) states. Here, we demonstrate a practical scheme to realize entangled measurements for *W* states. Thanks to the cyclic shift symmetry in the discrete Fourier transformation (DFT) of bosonic modes, the DFT measurement outcomes can be used to deterministically project multiqubit states onto *W* states. Experimentally, we show that three-qubit *W* state discrimination can be achieved by detecting the cyclic shift symmetry with a three-mode DFT optical circuit, yielding a measurement discrimination fidelity of 0.871 ± 0.039. Our experimental demonstration opens the door for the development of new quantum network protocols between multipartite systems.

INTRODUCTION

The efficient generation, evaluation, and estimation of multipartite entanglements is of great importance in the rapidly developing field of quantum information technology (*1*–*3*). In particular, quantum computing technologies rely on complex multipartite entanglement generated and controlled by a network of quantum gates, the effects of which can only be observed using local qubit readouts (*4*). Multipartite entanglement also plays a central role in error correction (*5*) and measurement-based quantum computation (*6*, *7*). On the other hand, the evaluation of multipartite entangled states by local qubit measurements is highly inefficient. The number of measurements required to reconstruct the complete density matrix of a system consisting of N qubits increases exponentially with N (*8*). In the case of photonic quantum computation, the situation is particularly difficult since most quantum gate operations can only be performed stochastically (*9*, *10*).

A more efficient evaluation of multipartite entanglement can be achieved by using entangled measurements (*11*). Entangled measurements are the measurements that cannot be represented by local measurement operators because they project the quantum system onto a specific set of entangled states (*12*). The best known example is the two-qubit case, where Bell measurements describe a projection on four orthogonal maximally entangled states (*13*–*15*) and have been used for quantum teleportation (*16*–*19*). Thus, multipartite entangled measurements for more than two qubits can enable more complex quantum teleportation protocols (*20*, *21*) and can facilitate complex operations in quantum networks (*22*, *23*). As pointed out by Gisin in a recent review (*24*), entangled measurement has so far received insufficient attention given its potential utility for quantum information technologies. Previous scalable implementations of multipartite entangled measurements focused exclusively on the class of entangled states known as Greenberger-Horne-Zeilinger (GHZ) states (*23*, *25*, *26*). While entangled measurement for four-qubit W states has been theoretically proposed (*27*), the proposed optical circuit lacks scalability for higher qubit numbers and has not been realized experimentally.

Here, we report the scalable implementation of an entangled measurement for W states (*28*, *29*). This class of states is identical to Dicke states associated with collective excitations of two-level systems and might represent a more natural form of multipartite entangled states than the GHZ states. W states are characterized by a nontrivial cyclic shift symmetry (CSS), where a cyclic exchange of the qubits corresponds to a cyclic shift of the N components of the W state in the local qubit basis. We propose an optical implementation of an entangled measurement for W states based on a pair of multiphoton measurements sensitive to the CSS of an N-mode system. As shown in previous work (*30*, *31*), such a measurement can be realized using a linear optics mode transformation corresponding to a discrete Fourier transform (DFT) of the N modes. In principle, this setup can detect a W state with 100% efficiency, a result that cannot be obtained when post-selected quantum gates are used for the same purpose.

Furthermore, an entangled measurement for three photonic qubits was demonstrated harnessing a specially designed stable interferometer (*31*–*34*) consisting of a hybrid beam splitter (HBS). We have successfully verified the realization of entangled measurements for W states with a measurement discrimination fidelity (MDF) of 0.871 ± 0.039. We believe that these results represent an important milestone toward a wider application of multi-qubit entangled measurements in photonic quantum computation, quantum communication, and sensing.

RESULTS

N-qubit *W* state

The W state is first introduced as an entangled quantum state of three qubits (*28*). For a photonic qubit encoded by polarization, the W state can be written as

$$|W_3\rangle = \frac{1}{\sqrt{3}}(|\mathrm{VHH}\rangle + |\mathrm{HVH}\rangle + |\mathrm{HHV}\rangle) \quad (1)$$

where $|\mathrm{H}\rangle$ and $|\mathrm{V}\rangle$ denote horizontal and vertical polarizations, respectively. There are also two other W states orthogonal to $|W_3\rangle$, as follows

$$\frac{1}{\sqrt{3}}\left(|\mathrm{VHH}\rangle + e^{-\mathrm{i}\frac{2\pi}{3}}|\mathrm{HVH}\rangle + e^{-\mathrm{i}\frac{4\pi}{3}}|\mathrm{HHV}\rangle\right) \quad (2)$$

[1]Department of Electronic Science and Engineering, Kyoto University, Kyotodaigakukatsura, Nishikyo-ku, Kyoto 615-8510, Japan. [2]Graduate School of Advanced Science and Engineering, Hiroshima University, Kagamiyama 1-3-1, Higashi Hiroshima 739-8530, Japan. [3]Photonic Quantum Sensing Science and Engineering Center, Graduate School of Engineering, Kyoto University, Kyoto 615-8510, Japan.
*Corresponding author. Email: takeuchi@kuee.kyoto-u.ac.jp

$$\frac{1}{\sqrt{3}}\left(|\mathrm{VHH}\rangle + e^{-\mathrm{i}\frac{4\pi}{3}}|\mathrm{HVH}\rangle + e^{-\mathrm{i}\frac{2\pi}{3}}|\mathrm{HHV}\rangle\right) \tag{3}$$

These three states form a set of orthogonal basis states, where one photonic qubit is $|\mathrm{V}\rangle$ and the other two states are $|\mathrm{H}\rangle$, and can be written in a unified way using a parameter $K = 0,1,2$

$$|W_3(K)\rangle = \frac{1}{\sqrt{3}}\sum_{m=0}^{2} e^{-\mathrm{i}\frac{2\pi}{3}m\cdot K}\left(\hat{S}_q\right)^m |\mathrm{VHH}\rangle \tag{4}$$

where $\hat{S}_q$ is a cyclic qubit-shift operator that acts on the ordered set of qubits by shifting each state of the mth qubit to the $(m+1)$th qubit. The cycle is closed by mapping the state of the last qubit back to the first qubit. For example, applying the cyclic qubit-shift operator twice to $|\mathrm{HHV}\rangle$ results in $\left(\hat{S}_q\right)^2|\mathrm{HHV}\rangle = \hat{S}_q|\mathrm{VHH}\rangle = |\mathrm{HVH}\rangle$.

The W state has been generalized for N qubits (*28*) and refers to the quantum superposition with equal probability amplitudes of all possible pure states in which exactly one of the qubits is $|\mathrm{V}\rangle$ and the others are in $|\mathrm{H}\rangle$

$$|W_N\rangle = \frac{1}{\sqrt{N}}(|\mathrm{VH}\cdots\mathrm{H}\rangle + |\mathrm{HV}\cdots\mathrm{H}\rangle + \cdots + |\mathrm{HH}\cdots\mathrm{V}\rangle) \tag{5}$$

Similar to the case of $N = 3$, the following states form a set of orthogonal basis states for the states where one photonic qubit is $|\mathrm{V}\rangle$ and the other $N-1$ qubits are $|\mathrm{H}\rangle$

$$|W_N(K)\rangle = \frac{1}{\sqrt{N}}\sum_{m=0}^{N-1} e^{-\mathrm{i}\frac{2\pi}{N}m\cdot K}\left(\hat{S}_q\right)^m |\mathrm{V}\overbrace{\mathrm{H}\cdots\mathrm{HH}}^{N-1}\rangle \tag{6}$$

where $K = 0,1,2, \ldots, N-1$. The state of Eq. 6 is the eigenstate of $\hat{S}_q$ with the eigenvalue of $e^{\mathrm{i}\frac{2\pi}{N}K}$, as follows

$$\hat{S}_q|W_N(K)\rangle = e^{\mathrm{i}\frac{2\pi}{N}K}|W_N(K)\rangle \tag{7}$$

Note that $|W_N(K)\rangle$ has CSS.

The choice of H polarization as the majority polarization is arbitrary. To apply the same logic for the states with V polarization as the majority polarization, we introduce $|\overline{W}(K)\rangle$ as the state in which H and V are exchanged,

$$|\overline{W}_N(K)\rangle = \frac{1}{\sqrt{N}}\sum_{m=0}^{N-1} e^{-\mathrm{i}\frac{2\pi}{N}m\cdot K}\left(\hat{S}_q\right)^m |\mathrm{H}\overbrace{\mathrm{V}\cdots\mathrm{VV}}^{N-1}\rangle \tag{8}$$

W state measurements using CSS

Here, we propose using the CSS of the W state to realize an entangled measurement that projects arbitrary N-photon inputs onto an orthogonal basis of the W states. As shown in Fig. 1, we accomplish this by first separating the vertically polarized photons from the horizontally polarized photons. This separation ensures that the total number of horizontally polarized and vertically polarized photons is reliably detected in the output ports, independent of the linear optics transformations applied to the paths. It is then possible to perform a measurement sensitive to the CSS in each of the N-mode systems (*30*, *31*).

This measurement is realized by a linear optics transformation of the input mode given by the DFT shown in Fig. 1B

$$\hat{b}_k^\dagger = \frac{1}{\sqrt{N}}\sum_{m=0}^{N-1} e^{-\mathrm{i}\frac{2\pi k}{N}m}\hat{a}_m^\dagger \tag{9}$$

where the photon creation operators $\hat{a}_m^\dagger$ represent the input modes and the creation operators $\hat{b}_k^\dagger$ represent the output modes $(k = 0, 1, \ldots, N-1)$ in which the photons will be detected. Each multiphoton detection event obtained with the DFT in place can be represented by the k values of the output modes in which the individual photons were detected, $\{k_j\}$ (*30*, *35*–*37*). For example, the DFT measurement outcome can be expressed in terms of the photon numbers as $|n_0 = 2, n_1 = 1, n_2 = 0\rangle$ when two photons, one photon, and no photon are detected in modes n_0, n_1, and n_2, respectively. Here, we describe this same state by using a sequence of k values of each of the three photons, with the rule that lower k value of photo will always be listed first. Since the first photon and the second photon are in the lowest output mode $k = 0$, and the third photon is in the output mode $k = 1$, we find $|\{k_j\}\rangle = |\{0,0,1\}\rangle$. Using the same logic, the state $|n_0 = 0, n_1 = 1, n_2 = 2\rangle$ can be written as $|\{k_j\}\rangle = |\{1,2,2\}\rangle$. The advantage of this expression is that the effects of a collective mode shift can now be expressed directly in terms of a sum of the individual k values,

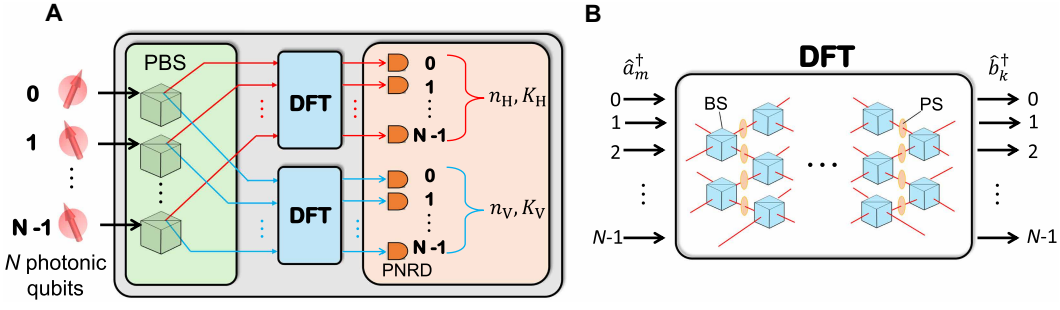

Fig. 1. *W* state measurement using CSS. (**A**) Schematic diagram of entangled measurement for W state in the photonic qubits encoded by polarization. PBS, polarizing beam splitter; DFT, discrete Fourier transformation; PNRD, photon number resolving detector. (**B**) Schematic diagram of N-mode DFT linear optical circuit: BS, beam splitter; PS, phase shifter.

$$\hat{S}\,|\{k_j\}\rangle = e^{-i\frac{2\pi}{N}\cdot\left(\sum_{j=1}^{N} k_j\right)}\,|\{k_j\}\rangle \tag{10}$$

where $\hat{S}$ is the cyclic-mode shift operator defined in (*30*). Each measurement outcome is therefore characterized by the total K value of its CSS.

In our measurement apparatus, we obtain two different values for horizontal and vertical polarization

$$\begin{aligned} K_{\mathrm{H}} &= \sum_{j=1}^{n_{\mathrm{H}}} k_{\mathrm{H}j} (\mathrm{mod} N) \\ K_{\mathrm{V}} &= \sum_{j=1}^{n_{\mathrm{V}}} k_{\mathrm{V}j} (\mathrm{mod} N) \end{aligned} \tag{11}$$

where n_{H} and n_{V} are the numbers of horizontal and vertical photons, respectively. Therefore, each measurement outcome characterizes the CSS of the N qubit input state according to

$$\hat{S}_q\,|\{k_{\mathrm{H}j}, k_{\mathrm{V}j}\}\rangle = e^{-i\frac{2\pi}{N}K}\,|\{k_{\mathrm{H}j}, k_{\mathrm{V}j}\}\rangle \tag{12}$$

where the total K value is given by

$$K = K_H + K_V (\mathrm{mod} N) \tag{13}$$

Since $|W_N(K)\rangle$ and $|\overline{W}_N(K)\rangle$ are characterized by a specific K value, they are orthogonal to measurement results with different K values. If only one photon is vertically polarized, the measurement projects the qubit state onto $|W_N(K)\rangle$. If only one photon is horizontally polarized, it projects the qubit state onto $|\overline{W}_N(K)\rangle$. The setup shown in Fig. 1 thus realizes an entangled measurement for the type of multi-qubit entanglement described by W states.

Because of the sensitivity to the K value, the measurement produces no false negatives. In other words, if the input state is $|W_N(K)\rangle$, the total probability of detecting the outcome $|W_N(K)\rangle$ is given by

$$\sum_{K_{\mathrm{H}}+K_{\mathrm{V}}=K} |\langle\{k_{\mathrm{H}j}, k_{\mathrm{V}j}\}|\,W_N(K)\rangle|^2 = 1 \tag{14}$$

where the sum runs over all combinations of $k_{\mathrm{H}j}$ and $k_{\mathrm{V}j}$ with a total value of K. The set of outcomes $\{k_{\mathrm{H}j}, k_{\mathrm{V}j}\}$ with $K_{\mathrm{H}} + K_{\mathrm{V}} = K$ is equivalent to a single projection onto the quantum state component $|W_N(K)\rangle$ with an efficiency of 1.

Consequently, the linear optical circuit for the entangled measurement combines the photon separation and DFT measurement processes depicted in Fig. 1. Initially, N polarization qubits are prepared along distinct paths. Each photon then passes through a polarizing BS (PBS), splitting into N paths for horizontal modes and N paths for vertical modes. The separated photons are injected into two DFT optical circuits. After the DFT optical circuit, all the photons are measured by photon number resolving detectors (PNRDs). Note that the photon separation by the PBSs and DFT measurement operators are compatible, meaning that their order can be interchanged without affecting the outcome. From the DFT measurement outcomes, the numbers of horizontal and vertical photons $(n_{\mathrm{H}}, n_{\mathrm{V}})$ can be determined. Specifically, the measurement outcomes $(n_{\mathrm{H}} = N-1, n_{\mathrm{V}} = 1)$ and $(n_{\mathrm{H}} = 1, n_{\mathrm{V}} = N-1)$ correspond to projection onto the W state bases $|W_N(K)\rangle$ and $|\overline{W}_N(K)\rangle$, respectively. The photon number distributions of DFT outcomes directly provide K_{H} and K_{V} as calculated from Eq. 11. Therefore, this linear optical circuit can distinguish between $2N$ orthogonal W state outcomes with an efficiency of 100%. For $N = 2$, this entangled measurement approach corresponds to the standard Bell-state measurement implemented by a balanced BS (*13*). In that case, a projection onto Bell states is obtained for $(n_{\mathrm{H}} = 1, n_{\mathrm{V}} = 1)$, discriminating between two orthogonal Bell states with $K = 0$ or $K = 1$, respectively. The present technique thus represents a generalization of Bell measurements to N-qubit states.

Testing *W* state entangled measurements using separable state inputs

In principle, an entangled measurement could be demonstrated by confirming that a specific W state input will be detected in the corresponding output channels. However, W states are difficult to generate and may have limited quantum state fidelities. Fortunately, it is possible to test measurements using completely separable states, which can be prepared with much higher fidelity. Similar to the verification of entanglement by local measurements, it is possible to verify that a measurement is entangled without using any entangled input states.

The key observation is that the components with one horizontally polarized qubit in a product state of local superpositions of $|\mathrm{H}\rangle$ and $|\mathrm{V}\rangle$ are in a coherent superposition that corresponds to a W state in that N dimensional subspace of the 2^N-dimensional N-qubit Hilbert space. The phases between the components can be controlled by local phase shifts. For three qubits, the state obtained from phase shifts of ϕ_0, ϕ_1, and ϕ_2 can be written as

$$\frac{1}{\sqrt{2}}\left(|\mathrm{H}\rangle + e^{i\phi_0}|\mathrm{V}\rangle\right) \otimes \frac{1}{\sqrt{2}}\left(|\mathrm{H}\rangle + e^{i\phi_1}|\mathrm{V}\rangle\right) \otimes \frac{1}{\sqrt{2}}\left(|\mathrm{H}\rangle + e^{i\phi_2}|\mathrm{V}\rangle\right) \tag{15}$$

This state can be expressed as a superposition of $|\mathrm{HHH}\rangle$, $|\mathrm{VVV}\rangle$, and two W states. For instance, when all local phases are set to zero, the state is given by the superposition

$$|\psi_0\rangle = \frac{1}{2\sqrt{2}}|\mathrm{HHH}\rangle + \frac{\sqrt{6}}{4}|W_3(0)\rangle + \frac{\sqrt{6}}{4}|\overline{W}_3(0)\rangle + \frac{1}{2\sqrt{2}}|\mathrm{VVV}\rangle \tag{16}$$

Each component of this superposition can be distinguished by the number of vertically polarized qubits n_{V}. Since the measurement apparatus shown in Fig. 1A correctly identifies the number of vertically polarized qubits, the entangled measurement should be able to identify the $|W_3(0)\rangle$ component for $n_{\mathrm{V}} = 1$ and the $|\overline{W}_3(0)\rangle$ component for $n_{\mathrm{V}} = 2$. Thus, demonstrating the projection onto $|W_3(0)\rangle$ and $|\overline{W}_3(0)\rangle$ is possible using the separable state input $|\psi_0\rangle$. By changing the phases with $(\phi_0, \phi_1, \phi_2) = \left(0, \frac{4\pi}{3}, \frac{2\pi}{3}\right)$, it is possible to demonstrate the projection onto $|W_3(1)\rangle$ and $|\overline{W}_3(2)\rangle$ with $|\psi_1\rangle$

$$|\psi_1\rangle = \frac{1}{2\sqrt{2}}|\mathrm{HHH}\rangle + \frac{\sqrt{6}}{4}W_3(1) + \frac{\sqrt{6}}{4}|\overline{W}_3(2)\rangle + \frac{1}{2\sqrt{2}}|\mathrm{VVV}\rangle \tag{17}$$

Furthermore, $|W_3(2)\rangle$ and $|\overline{W}_3(1)\rangle$ can be demonstrated from $|\psi_2\rangle$ by implementing a phase shift of $(\phi_0, \phi_1, \phi_2) = \left(0, \frac{2\pi}{3}, \frac{4\pi}{3}\right)$

$$|\psi_2\rangle = \frac{1}{2\sqrt{2}}|\mathrm{HHH}\rangle + \frac{\sqrt{6}}{4}|W_3(2)\rangle + \frac{\sqrt{6}}{4}|\overline{W}_3(1)\rangle + \frac{1}{2\sqrt{2}}|\mathrm{VVV}\rangle \tag{18}$$

The separable input states shown in Eqs. 16 to 18 contain all W state components.

In summary, the reason we are able to test the performance of W state measurement using these three separable input states is because the measurement apparatus we proposed can identify the number of horizontally or vertically polarized qubits, n_H and n_V and the K values, K_H and K_V, in the input state, simultaneously. Using this simultaneous measurement of polarization and K values, the entanglement of our measurement can be demonstrated using the three separable input states given in Eq. 18, where a polarization measurement of two horizontally polarized photons and one vertically polarized photon uniquely identifies the components $|W_3(K)\rangle$ and the measurement of one horizontally polarized photon and two vertically polarized photons identifies $|\overline{W}_3(K)\rangle$.

Experimental demonstration

Figure 2A shows the schematic setup of a three-qubit entangled measurement for W states. As explained in the previous section, three single-photon inputs are prepared in one of the qubit states in Eqs. 16 to 18. The three single-photon inputs pass through a three-mode DFT optical circuit, which can be decomposed as two balanced BSs (BS1 and BS3), a one-third reflectance of a BS (BS2), and a $\frac{\pi}{2}$ phase shifter (*31*, *38*). Note that if these DFT components are nonpolarizing, the two DFT circuits for horizontal and vertical modes in Fig. 1 can be implemented by a single (nonpolarizing) DFT circuit, ensuring stable operation of the entangled measurement (*31*, *34*). After the output of the DFT circuit is separated into two polarization modes by PBSs, the number of photons in six output modes is measured by PNRDs.

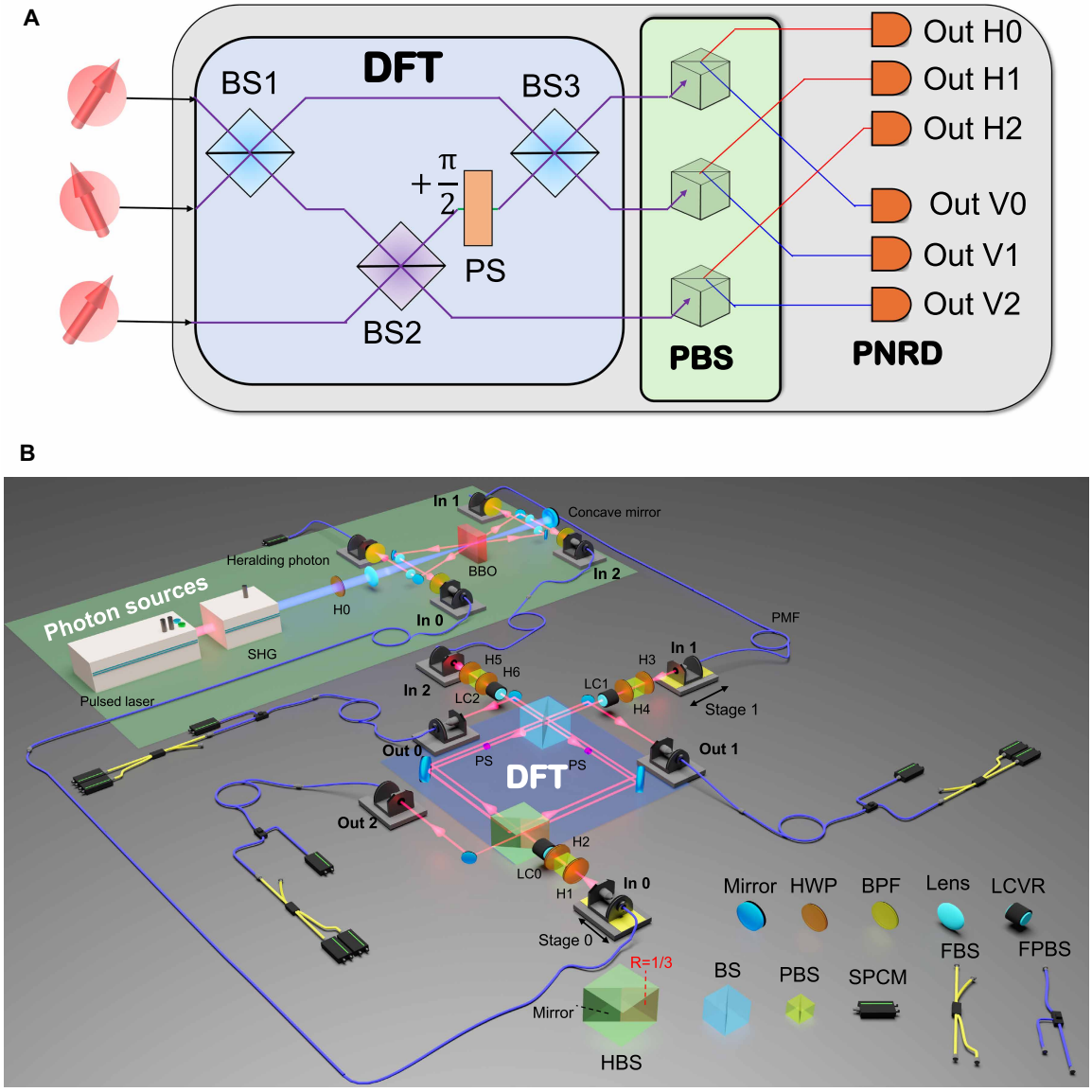

Fig. 2. Experimental setup. (**A**) Schematic setup for three-qubit entangled measurement for a W state. (**B**) Experimental setup for the evaluation of a W state entangled measurement. BBO, beta-barium borate; BPF, band-pass filter (780 ± 1 nm); SPCM, single photon counting module; HBS, hybrid BS; LCVR, liquid crystal variable retarder; FPBS, fiber PBS; PMF, polarization-maintaining fiber; SHG, second harmonic generation.

Figure 2B shows the actual experimental setup. Four single photons are generated via two forward and backward spontaneous parametric down-conversion (SPDC) processes pumped by a femtosecond-pulsed laser (see Materials and Methods). One of the four single photons is used for heralding the preparation of three single-photon inputs (*34*). To prepare the desired input state in Eqs. 16 to 18, each photon's polarization is purified and prepared for diagonal polarization using a set of half wave plates and PBSs, and then the phase between horizontal and vertical polarization is controlled by a liquid crystal variable retarder.

One of the challenges for the experimental implementation is that the optical path-length differences of the three-mode DFT in Fig. 2A have to be stabilized on the order of a few nanometers for stable operation. To solve this problem, we adopted a displaced-Sagnac architecture consisting of an HBS, in which a perfect mirror and a BS with a reflectance of one-third are integrated, and a balanced BS (see Materials and Methods). The constructed DFT photonic circuit is stable for hours without any active control of the optical paths.

The photon in each output mode of the DFT circuit is then coupled to fiber PBSs. One polarization mode is monitored by a PNRD consisting of two single-photon counting modules (SPCMs) coupled by an FBS, and the other polarization mode is detected by a single SPCM. To verify the entangled measurement for $|W_3(K)\rangle$, where one photonic qubit is $|\mathrm{V}\rangle$ and the other two are $|\mathrm{H}\rangle$, the horizontal polarization mode is monitored by the PNRD, while for $|\overline{W}_3(K)\rangle$ the vertical mode is monitored. Note that this is due to the limited experimental resources, and $|W_3(K)\rangle$ and $|\overline{W}_3(K)\rangle$ could be simultaneously detected using PNRDs for both of the polarization modes. All fourfold coincidence detection signals, including the heralding signal, are collected by a time-to-digital converter (DPC230, Becker & Hickl GmbH). The total coincidence counts of each measurement are set to around 500 counts. The brightness of the four-photon coincidence measurement is about 0.06 ~ 0.07 counts/s. We determine the probabilities from the collected coincidence counts by dividing the counts for each measurement basis by the total coincidence counts.

The ideal and experimentally obtained detection-probability distributions over the output modes of the DFT circuit are illustrated in Fig. 3. Specifically, Fig. 3A shows the ideal detection-probability distributions for $|W_3(0)\rangle$ where the three single-photon inputs are set to $|\psi_0\rangle$ in Eq. 16. For instance, the leftmost red bar represents the probability (≈ 0.22) of finding two photons in horizontal polarization mode 0 ($|200\rangle_{\mathrm{H}}$) and one photon in the vertical polarization mode 0 ($|100\rangle_{\mathrm{V}}$). From Eq. 11, $K_{\mathrm{H}} = 0$ for the states $|200\rangle_{\mathrm{H}}$ and $|011\rangle_{\mathrm{H}}$, and $K_{\mathrm{V}} = 0$ for $|100\rangle_{\mathrm{V}}$. The total $K = K_{\mathrm{H}} + K_{\mathrm{V}} = 0(\mathrm{mod}3)$ is the signature for the input state $|\psi_0\rangle$, which only contains the W state component $|W_3(0)\rangle$ from Eq. 16. Similarly, we can easily confirm that the detection probabilities for the total $K = 0$ (colored red) are nonzero in Fig. 3A, while the total $K = 1$ (blue) and $K = 2$ (green) are completely suppressed. Figure 3 (B and C) shows the ideal detection-probability distributions for W state components $|W_3(1)\rangle$ and $|W_3(2)\rangle$ when the input states are $|\psi_1\rangle$ and $|\psi_2\rangle$, respectively. In each case, the detection probabilities are nonzero only for $K = 1$ and $K = 2$, respectively.

Figure 3D displays the experimental result obtained with the input state prepared in $|\psi_0\rangle$. The most important point of this result is that, similar to the ideal distributions shown in Fig. 3A, only output patterns with total $K = 0$ (colored red) are observed with substantial probabilities, whereas outputs with total $K = 1$ or $K = 2$ are rarely detected. This result shows that our experimental setup can identify the W state component of $|W_3(0)\rangle$ with very high probability. The experimental results for the input states $|\psi_1\rangle$ and $|\psi_2\rangle$ are shown in Fig. 3 (E and F), where output detection patterns with total $K = 1$ (blue) and $K = 2$ (green), respectively, are observed with substantial probabilities. These results also indicate that the W state components of $|W_3(1)\rangle$ and $|W_3(2)\rangle$ can be distinguished by our experimental setup.

The ideal and experimentally obtained detection-probability distributions for $|\overline{W}_3(K)\rangle$ where one photonic qubit is $|\mathrm{H}\rangle$ and the other two are $|\mathrm{V}\rangle$ are depicted in Fig. 3 (G to I) and (J to L), respectively. Note that for this measurement, PNRDs are used to detect vertical polarization modes. The leftmost red bar in Fig. 3G shows the probability of finding two photons in the vertical polarization mode 0 ($|200\rangle_{\mathrm{V}}$) and one photon in the horizontal polarization mode 0 ($|100\rangle_{\mathrm{H}}$). Similar to the results for $|W_3(K)\rangle$, the probability bars are colored red, blue, and green for total K values of 0, 1, and 2, respectively. Note that, as indicated in Eqs. 17 and 18, the input states $|\psi_2\rangle$ and $|\psi_1\rangle$ have $|\overline{W}_3(1)\rangle$ and $|\overline{W}_3(2)\rangle$, respectively, contrasting with the verification of $|W_3(1)\rangle$ and $|W_3(2)\rangle$. As shown in Fig. 3 (J to L), only those output patterns with a total K value matching the expected W state component of $|\overline{W}_3(K)\rangle$ have substantial probabilities, while other patterns are rarely observed. These results show that our entangled measurement setup can identify the W state component of $|\overline{W}_3(K)\rangle$ with very high probability. Details on the cause of the discrepancy between the ideal and experimental distributions will be given later.

Next, we evaluate the MDF (*14*, *15*, *39*), which is the probability of correctly detecting W state components for a given input state, from the experimentally obtained detection-probability distributions shown in Fig. 3. Figure 4A shows the sum of probabilities for a certain total K value calculated from the distributions shown in Fig. 3 (D to F). For the input state $|\psi_0\rangle$, the MDF for $|W_3(0)\rangle$ is 0.882 ± 0.038, indicating that the realized entangled measurement can discriminate the W state component $|W_3(0)\rangle$ with a probability of 88.2%. The MDF for W state components $|W_3(K)\rangle$ is obtained as 0.871 ± 0.039, given by the average of the MDF for the corresponding total K values. Similarly, the MDF for W state components $|\overline{W}_3(K)\rangle$ is obtained as 0.870 ± 0.038. Accordingly, the averaged MDF is 0.871 ± 0.039. Since the averaged MDF exceeds the maximal MDF of two-thirds achievable by a bi-separable measurement, we conclude that the entangled measurement for three-qubit W states has been successfully demonstrated.

Since an MDF of one can only be achieved by a measurement projection onto a W state corresponding to the detected polarizations, the MDF provides a very good estimate of the fidelity of our entangled measurement. To illustrate this point, it may be useful to consider the possible application of our entangled measurement to remote state preparation, where one qubit each from three maximally entangled qubit pairs is input into our measurement device. Ideally, the projection on a W state then prepares a corresponding W state in the remote qubits, where the entanglement between qubits from different pairs can only be generated because the measurement performed on the other three qubits is entangled. We can now use the MDF determined with the separable input state in Eq. 16 to predict the fidelity of remote state preparation. In the absence of other

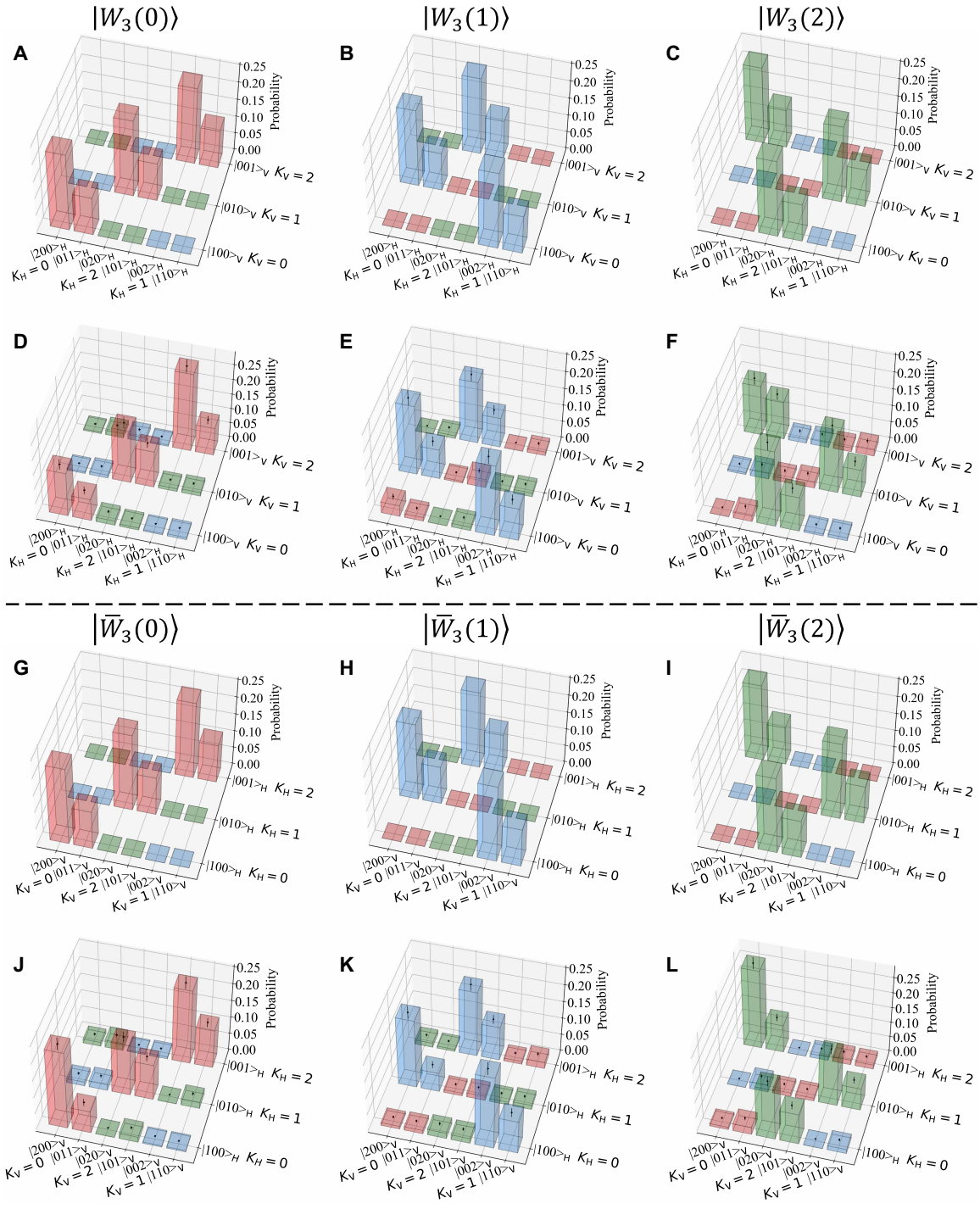

Fig. 3. Experimental results for *K* value correlation tables. (**A**) to (**C**) show the ideal detection-probability distributions for $|W_3(0)\rangle$, $|W_3(1)\rangle$, and $|W_3(2)\rangle$, respectively. (**D**) to (**F**) show the experimentally obtained detection-probability distributions for $|W_3(0)\rangle$, $|W_3(1)\rangle$, and $|W_3(2)\rangle$, respectively. (**G**) to (**I**) show the ideal detection-probability distributions for $|\overline{W}_3(0)\rangle$, $|\overline{W}_3(1)\rangle$, and $|\overline{W}_3(2)\rangle$, respectively. (**J**) to (**L**) show the experimentally obtained detection-probability distributions for $|\overline{W}_3(0)\rangle$, $|\overline{W}_3(1)\rangle$, and $|\overline{W}_3(2)\rangle$, respectively. The total *K* value is obtained as $K = K_H + K_V (\mathrm{mod} 3)$. The red, blue, and green bars indicate the total *K* values of zero, one, and two, respectively.

errors, this fidelity is expected to be given by the MDF, illustrating the conceptual relation between entangled measurements and entangled states.

DISCUSSION

We have presented a scalable implementation of an entangled measurement for W states. In our scheme, W states are characterized by a nontrivial CSS. We proposed an optical implementation of the entangled measurement for W states using DFT circuit. Experimentally, we verified an entangled measurement system for three photonic qubits using an ultrastable displaced-Sagnac interferometer consisting of HBSs. We achieved an averaged MDF of 0.871 ± 0.039, showing the successful realization of entangled measurement for W states.

The cause of the observed error between the ideal and experimental results can be attributed to the state preparation and imperfections in the constructed entangled measurement for W states. For example, simultaneous generation of more than three-photon pairs, timing jitters of the pulse excitation of different crystals (*40*), and the nonperfect indistinguishability of the single photons due to spatiotemporal mismatch (*41*) are possible causes of the errors in the state preparation. Imperfections in the realized entangled measurement may include polarization-dependent phase shifts in the optical components.

The entangled measurement for W states developed here opens several promising avenues for quantum information applications. For instance, it enables multiparty measurement-device–independent quantum key distribution (*27*). Furthermore, this technique provides a powerful tool for entanglement swapping protocols, as demonstrated in GHZ states (*25*, *26*), representing a fundamental advantage for scalable quantum networks (*42*).

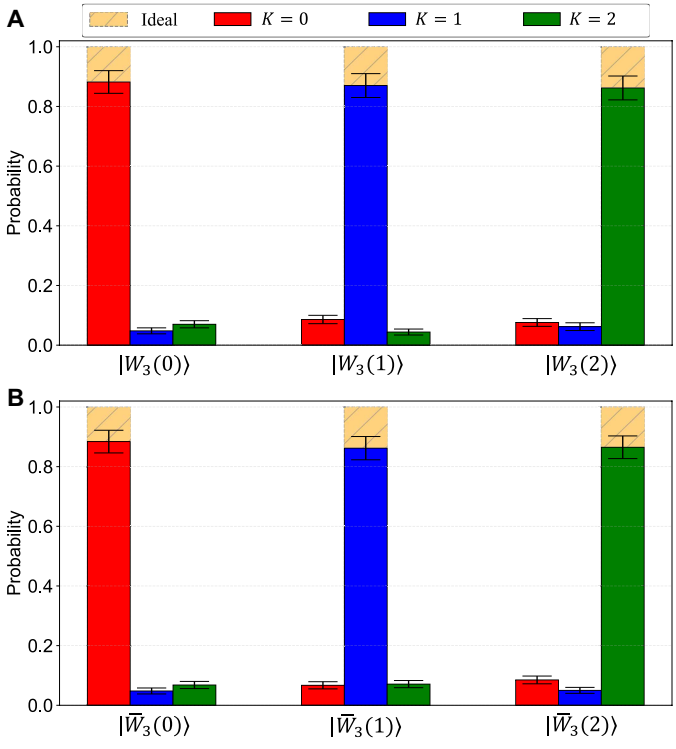

Fig. 4. Sum of probabilities for identical *K* values. (**A**) and (**B**) correspond to W state components $|W_3(K)\rangle$ and $|\overline{W}_3(K)\rangle$, respectively. For the input state $|\psi_0\rangle$, the MDFs of $|W_3(0)\rangle$ and $|\overline{W}_3(0)\rangle$ are obtained as 0.882 ± 0.038 and 0.884 ± 0.038. For the $|\psi_1\rangle$, the MDFs of $|W_3(1)\rangle$ and $|\overline{W}_3(2)\rangle$ are 0.870 ± 0.040 and 0.865 ± 0.038. For $|\psi_1\rangle$, the MDFs of $|W_3(2)\rangle$ and $|\overline{W}_3(1)\rangle$ are 0.862 ± 0.040 and 0.861 ± 0.039.

MATERIALS AND METHODS

Sagnac architecture of a three-mode DFT optical circuit

Figure 5 shows a schematic diagram of a three-mode DFT optical circuit. As discussed in Results, the three-mode DFT can be decomposed into two balanced BSs, a one-third reflection ratio BS, and a +π/2 phase shifter (*38*), as depicted in Fig. 5A. One of the challenges for the experimental implementation is that the optical path-length differences of the two optical modes colored red and blue in Fig. 5A have to be stabilized on the order of a few nanometers for stable operation. To solve this problem, we adopted a displaced-Sagnac architecture consisting of an HBS, in which a perfect mirror and a BS with a reflectance of one-third are integrated, and a balanced BS. In this architecture, the two optical modes colored

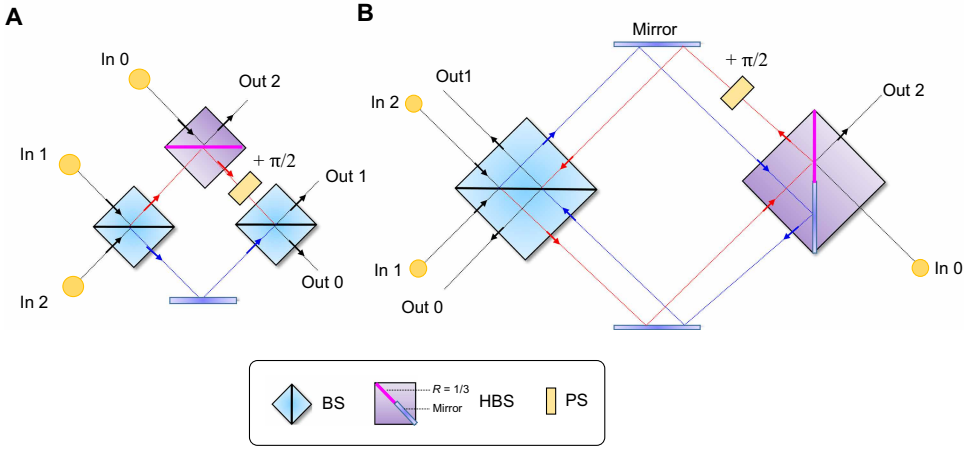

Fig. 5. Schematic diagram of three-mode discrete DFT optical circuit. (**A**) Original method to construct DFT. (**B**) Sagnac architecture DFT.

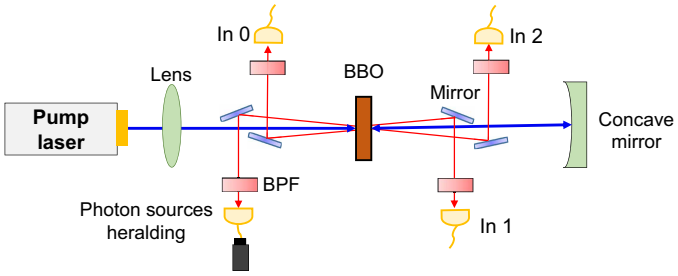

Fig. 6. Schematic setup for photon sources.

red and blue in Fig. 5B pass through all optical elements, providing long-term stability.

SPDC photon sources

Figure 6 shows a schematic setup for photon sources. A pump pulse (82 MHz @390 nm) passes through a 1.6-mm-thick type I beta-barium borate crystal twice to generate two pairs of photons. Subsequently, these photons are directed to narrow band-pass filters (centered at 780 nm with a full width at half maximum of 2 nm) and collected into polarization-maintaining fibers. In 0, In 1, and In 2 refer to the input ports of the DFT optical circuit.

REFERENCES AND NOTES

1. J.-W. Pan, Z.-B. Chen, C.-Y. Lu, H. Weinfurter, A. Zeilinger, M. Ż. Żukowski, Multiphoton entanglement and interferometry. *Rev. Mod. Phys.* **84**, 777–838 (2012).
2. R. Horodecki, P. Horodecki, M. Horodecki, K. Horodecki, Quantum entanglement. *Rev. Mod. Phys.* **81**, 865–942 (2009).
3. S. Cao, B. Wu, F. Chen, M. Gong, Y. Wu, Y. Ye, C. Zha, H. Qian, C. Ying, S. Guo, Q. Zhu, H.-L. Huang, Y. Zhao, S. Li, S. Wang, J. Yu, D. Fan, D. Wu, H. Su, H. Deng, H. Rong, Y. Li, K. Zhang, T.-H. Chung, F. Liang, J. Lin, Y. Xu, L. Sun, C. Guo, N. Li, Y.-H. Huo, C.-Z. Peng, C.-Y. Lu, X. Yuan, X. Zhu, J.-W. Pan, Generation of genuine entanglement up to 51 superconducting qubits. *Nature* **619**, 738–742 (2023).
4. M. A. Nielsen, I. L. Chuang, *Quantum computation and quantum information* (Cambridge Univ. Press, 2010).
5. S. J. Devitt, W. J. Munro, K. Nemoto, Quantum error correction for beginners. *Rep. Prog. Phys.* **76**, 076001 (2013).
6. H. J. Briegel, R. Raussendorf, Persistent entanglement in arrays of interacting particles. *Phys. Rev. Lett.* **86**, 910–913 (2001).
7. I. Schwartz, D. Cogan, E. R. Schmidgall, Y. Don, L. Gantz, O. Kenneth, N. H. Lindner, D. Gershoni, Deterministic generation of a cluster state of entangled photons. *Science* **354**, 434–437 (2016).
8. D. F. V. James, P. G. Kwiat, W. J. Munro, A. G. White, Measurement of qubits. *Phys. Rev. A* **64**, 052312 (2001).
9. E. Knill, R. Laflamme, G. J. Milburn, A scheme for efficient quantum computation with linear optics. *Nature* **409**, 46–52 (2001).
10. P. Kok, W. J. Munro, K. Nemoto, T. C. Ralph, J. P. Dowling, G. J. Milburn, Linear optical quantum computing with photonic qubits. *Rev. Mod. Phys.* **79**, 135–174 (2007).
11. N. Friis, G. Vitagliano, M. Malik, M. Huber, Entanglement certification from theory to experiment. *Nat. Rev. Phys.* **1**, 72–87 (2019).
12. F. Del Santo, J. Czartowski, K. Ż. Życzkowski, N. Gisin, Iso-entangled bases and joint measurements. *Phys. Rev. Res.* **6**, 023085 (2024).
13. M. Michler, K. Mattle, H. Weinfurter, A. Zeilinger, Interferometric bell-state analysis. *Phys. Rev. A* **53**, R1209–R1212 (1996).
14. N. B. Lingaraju, H.-H. Lu, D. E. Leaird, S. Estrella, J. M. Lukens, A. M. Weiner, Bell state analyzer for spectrally distinct photons. *Optica* **9**, 280–283 (2022).
15. M. J. Bayerbach, S. E. D'Aurelio, P. van Loock, S. Barz, Bell-state measurement exceeding 50% success probability with linear optics. *Sci. Adv.* **9**, eadf4080 (2023).
16. C. H. Bennett, G. Brassard, C. Crépeau, R. Jozsa, A. Peres, W. K. Wootters, Teleporting an unknown quantum state via dual classical and einstein-podolsky-rosen channels. *Phys. Rev. Lett.* **70**, 1895–1899 (1993).
17. D. Bouwmeester, J.-W. Pan, K. Mattle, M. Eibl, H. Weinfurter, A. Zeilinger, Experimental quantum teleportation. *Nature* **390**, 575–579 (1997).
18. A. Furusawa, J. L. Sørensen, S. L. Braunstein, C. A. Fuchs, H. J. Kimble, E. S. Polzik, Unconditional quantum teleportation. *Science* **282**, 706–709 (1998).
19. S. Pirandola, J. Eisert, C. Weedbrook, A. Furusawa, S. L. Braunstein, Advances in quantum teleportation. *Nat. Photonics* **9**, 641–652 (2015).
20. J. Joo, Y.-J. Park, S. Oh, J. Kim, Quantum teleportation via a w state. *New J. Phys.* **5**, 136 (2003).
21. P. Agrawal, A. Pati, Perfect teleportation and superdense coding with *w* states. *Phys. Rev. A* **74**, 062320 (2006).
22. M. Murao, D. Jonathan, M. B. Plenio, V. Vedral, Quantum telecloning and multiparticle entanglement. *Phys. Rev. A* **59**, 156–161 (1999).
23. N.-N. Wang, A. Pozas-Kerstjens, C. Zhang, B.-H. Liu, Y.-F. Huang, C.-F. Li, G.-C. Guo, N. Gisin, A. Tavakoli, Certification of non-classicality in all links of a photonic star network without assuming quantum mechanics. *Nat. Commun.* **14**, 2153 (2023).
24. N. Gisin, Entanglement 25 years after quantum teleportation: Testing joint measurements in quantum networks. *Entropy* **21**, 325 (2019).
25. J.-w. Pan, A. Zeilinger, Greenberger-Horne-Zeilinger-state analyzer. *Phys. Rev. A* **57**, 2208–2211 (1998).
26. C.-Y. Lu, T. Yang, J.-W. Pan, Experimental multiparticle entanglement swapping for quantum networking. *Phys. Rev. Lett.* **103**, 020501 (2009).
27. C. Zhu, F. Xu, C. Pei, W-state analyzer and multi-party measurement-device-independent quantum key distribution. *Sci. Rep.* **5**, 17449 (2015).
28. W. Dür, G. Vidal, J. I. Cirac, Three qubits can be entangled in two inequivalent ways. *Phys. Rev. A* **62**, 062314 (2000).
29. T. Tashima, T. Wakatsuki, Ş. K. Özdemir, T. Yamamoto, M. Koashi, N. Imoto, Local transformation of two einstein-podolsky-rosen photon pairs into a three-photon *W* state. *Phys. Rev. Lett.* **102**, 130502 (2009).
30. J.-Y. Wu, H. F. Hofmann, Evaluation of bipartite entanglement between two optical multi-mode systems using mode translation symmetry. *New J. Phys.* **19**, 103032 (2017).
31. T. Kiyohara, N. Yamashiro, R. Okamoto, H. Araki, J.-Y. Wu, H. F. Hofmann, S. Takeuchi, Direct and efficient verification of entanglement between two multimode-multiphoton systems. *Optica* **7**, 1517–1523 (2020).
32. R. Okamoto, J. L. O'Brien, H. F. Hofmann, T. Nagata, K. Sasaki, S. Takeuchi, An entanglement filter. *Science* **323**, 483–485 (2009).
33. R. Okamoto, J. L. O'Brien, H. F. Hofmann, S. Takeuchi, Realization of a Knill-Laflamme-Milburn controlled-not photonic quantum circuit combining effective optical nonlinearities. *Proc. Natl. Acad. Sci.* **108**, 10067–10071 (2011).
34. G. Park, I. Matsumoto, T. Kiyohara, H. F. Hofmann, R. Okamoto, S. Takeuchi, Realization of photon correlations beyond the linear optics limit. *Sci. Adv.* **9**, eadj8146 (2023).
35. M. C. Tichy, M. Tiersch, F. de Melo, F. Mintert, A. Buchleitner, Zero-transmission law for multiport beam splitters. *Phys. Rev. Lett.* **104**, 220405 (2010).
36. C. Dittel, G. Dufour, M. Walschaers, G. Weihs, A. Buchleitner, R. Keil, Totally destructive many-particle interference. *Phys. Rev. Lett.* **120**, 240404 (2018).
37. C. Dittel, G. Dufour, M. Walschaers, G. Weihs, A. Buchleitner, R. Keil, Totally destructive interference for permutation-symmetric many-particle states. *Phys. Rev. A* **97**, 062116 (2018).
38. M. Reck, A. Zeilinger, H. J. Bernstein, P. Bertani, Experimental realization of any discrete unitary operator. *Phys. Rev. Lett.* **73**, 58–61 (1994).
39. S. Wein, K. Heshami, C. A. Fuchs, H. Krovi, Z. Dutton, W. Tittel, C. Simon, Efficiency of an enhanced linear optical bell-state measurement scheme with realistic imperfections. *Phys. Rev. A* **94**, 032332 (2016).
40. M. Tanida, R. Okamoto, S. Takeuchi, Highly indistinguishable heralded single-photon sources using parametric down conversion. *Opt. Express* **20**, 15275–15285 (2012).
41. T. Nagata, R. Okamoto, H. F. Hofmann, S. Takeuchi, Analysis of experimental error sources in a linear-optics quantum gate. *New J. Phys.* **12**, 043053 (2010).
42. J. Miguel-Ramiro, F. Riera-Sàbat, W. Dür, Quantum repeater for *W* states. *PRX Quantum* **4**, 040323 (2023).

Acknowledgments

Funding: This work was supported in part by ERATO, Japan Science and Technology Agency (JPMJER2402), MEXT Q-LEAP grant number JPMXS0118067634, JST-CREST grant Number JPMJCR1674, JSPS KAKENHI grant Number 21H04444 and 24H00195, WISE Program, MEXT, and the Research Fellow of Japan Society for the Promotion of Science (no. 22 J14998). **Author contributions:** S.T. supervised the research. G.P. and H.F.H. developed the theory and carried out the theoretical calculations. G.P. performed the experiment. All authors analyzed the data and wrote the manuscript with input from all authors. **Competing interests:** The authors declare that they have no competing interests. **Data and materials availability:** All data needed to evaluate the conclusions in the paper are present in the paper.

Submitted 12 March 2025
Accepted 11 August 2025
Published 12 September 2025
10.1126/sciadv.adx4180